Physica Medica 60 (2019) 76–82

Contents lists available at ScienceDirect

Physica Medica

journal homepage: www.elsevier.com/locate/ejmp

Original paper

T2, T2* and spin coupling ratio as biomarkers for the study of lipomatous tumors

Katerina Nikiforaki[a,b,*], Georgios C. Manikis[a,b], Eleftherios Kontopodis[a,b], Eleni Lagoudaki[c], Eelco de Bree[d], Kostas Marias[a,e], Apostolos H. Karantanas[a,b], Thomas G. Maris[b]

[a] Computational BioMedicine Laboratory, Institute of Computer Science, Foundation for Research and Technology-Hellas (FORTH), Heraklion, Crete, Greece
[b] Department of Radiology, University of Crete, Heraklion, Crete, Greece
[c] Department of Pathology, University Hospital of Crete, Heraklion, Crete, Greece
[d] Department of Surgical Oncology, University of Crete, Heraklion, Crete, Greece
[e] Technological Educational Institute of Crete, Department of Informatics Engineering, Heraklion, Crete, Greece

ARTICLE INFO

Keywords:
MR diagnosis
Tumors/lipomatous
Spin coupling ratio/biomarker
T2 relaxometry
T2* relaxometry

ABSTRACT

Background: Subcutaneous fat may have variable signal intensity on T2w images depending on the choice of imaging parameters. However, fatty components within tumors have a different degree of signal dependence on the acquisition scheme. This study examined the use of T2, T2* relaxometry and spin coupling related signal changes (Spin Coupling ratio, SCr) on two different imaging protocols as clinically relevant descriptors of benign and malignant lipomatous tumors.

Materials and methods: 20 patients with benign lipomas or liposarcomas of variable histologic grade were examined at an 1.5 T scanner with Multi Echo Spin Echo (MESE) different echo spacing (ESP) in order to produce bright fat T2w images (ESP: 13.4 ms, 25 equidistant echoes) and dark fat images (ESP: 26.8 ms with 10 equidistant echoes). T2* relaxometry acquisition comprises 4 sets of in-opposed echoes (2.4–19.2 ms, ESP: 2.4 ms) Multi Echo Gradient Echo (MEGRE) sequence. All parametric maps were calculated on a pixel basis.

Results: Significant differences of SCr were found for five different types of lipomatous tumors (Pairwise *t*-test with Bonferroni correction): lipomas, well differentiated liposarcomas, myxoid liposarcomas, pleomorphic liposarcomas and poorly differentiated liposarcomas. SCr surpassed the classification performance of T2 and T2* relaxometry.

Data conclusion: A novel biomarker based on spin coupling related signal loss, SCr, is indicative of lipomatous tumor histological grading. We concluded that T2, T2* and SCr can be used for the classification of fat containing tumors, which may be important for biopsy guidance in heterogeneous masses and treatment planning.

1. Introduction

Fat containing tumors can be benign (lipomas) or malignant (liposarcomas). Liposarcomas which account for approximately 20% of all sarcomas comprise different degrees of malignancy, including low (well differentiated), intermediate (myxoid) and high (pleomorphic, dedifferentiated) [1]. Histologic type and grade is important to predict the clinical behavior of liposarcomas, i.e. rate of growth, possibility to metastasize, risk of recurrence and survival rate.

Preoperative diagnosis of soft tissue tumor type and grade is essential for treatment planning. In the case of a malignant soft tissue tumor (sarcoma) wide excision of the tumor together with a rim of adjacent structures is the surgical treatment of choice to reduce the risk of involved margins and local recurrence, while in the case of a benign tumor marginal resection is adequate. Marginal resection is preferred where appropriate since it decreases the risk of short-term, functional and cosmetic morbidity, which are frequently observed after wide tumor excision. Moreover, depending on the exact tumor type and grade preoperative radiotherapy or chemotherapy may be indicated.

While MRI is the imaging method of choice for soft tissue tumors, unfortunately as yet reliable preoperative diagnosis is only accomplished by core needle or open biopsy. Since soft tissue tumors may be heterogeneous and the area with the highest malignancy grade determines its biological behavior, it is essential to harvest tissue samples from this site of the tumor. MRI may determine this specific area and consequently be helpful in directing the biopsy, either performed

* Corresponding author.
E-mail address: nikiforakik@gmail.com (K. Nikiforaki).

https://doi.org/10.1016/j.ejmp.2019.03.023
Received 15 February 2019; Received in revised form 19 March 2019; Accepted 21 March 2019
Available online 28 March 2019

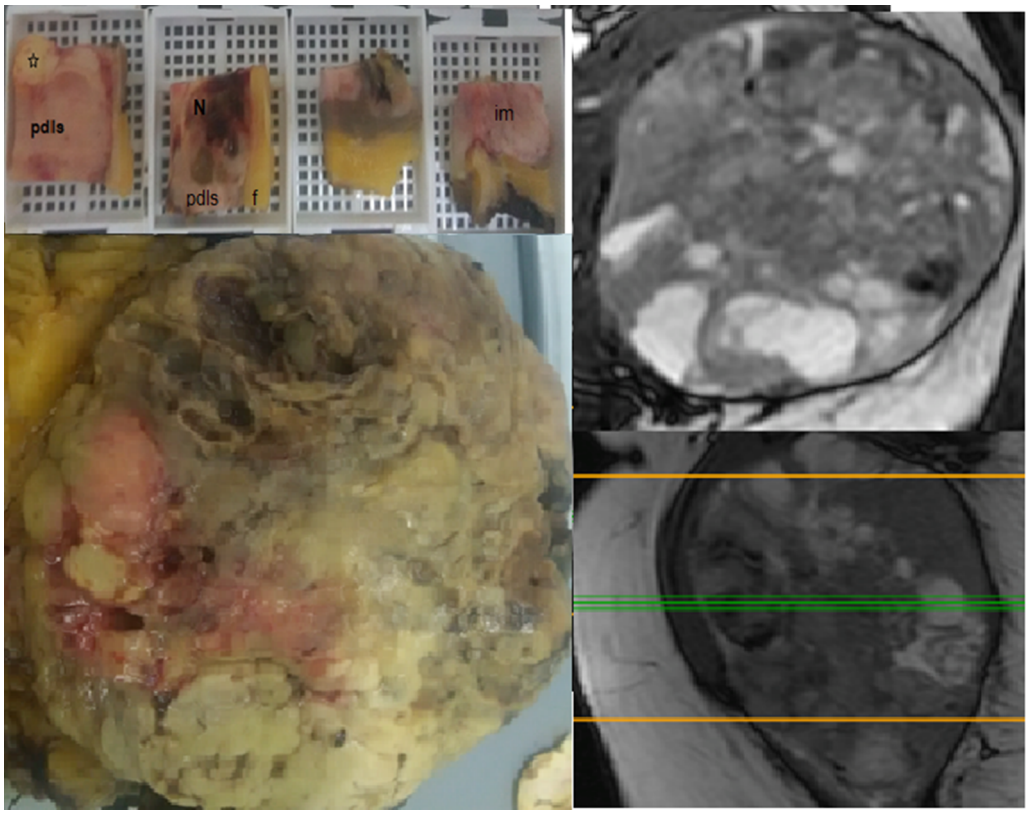

Fig. 1. Surgical specimen (dedifferentiated liposarcoma of the thigh). The central slice was divided into 26 orthogonal sections. Area of well differentiated liposarcoma (asterisk) is adjacent to area of poor differentiation (pdls). Necrotic (N), hemorrhagic areas and fat (f) were identified as well as infiltrated muscle (im). Corresponding axial and coronal T2/T1-w (trueFISP) images are shown on the right.

imaging-guided or by palpation. However, non-invasive achievement of the correct assessment of soft tissue tumor type and grade would avoid the potential complications of a biopsy, such as spillage of tumor cells, wound breakdown with tumor growth through the wound, pain, bleeding, wound infection and patient's discomfort. Moreover, since the vast majority of patients with a soft tissue tumor undergoes nevertheless MRI, additional costs of preoperative biopsy and histological examination may be saved. Hence, it would be a great accomplishment when type and grade of soft tissue tumors, including lipomatous tumors, and their heterogeneous areas can be determined in a non-invasive manner by MRI techniques.

Benign and malignant tumors of lipomatous origin can share a number of overlapping imaging characteristics on conventional MRI. Radiological diagnosis is based on lesion size, depth, presence of enhancing septa, etc. [2,3]. However tissue histopathological sample examination is needed to assess parameters as cell type, cellular atypia, number of mitoses and presence of necrosis for definitive tumor characterization.

However, apart from conventional MRI, quantitative biomarkers derived from an extended protocol can non-invasively offer an insight into tissue that can support radiological diagnosis. In this study we examined 2 widely used biomarkers and we introduce a novel biomarker related to spin coupling (Spin Coupling ratio, SCr).

T2 relaxometry has been a robust and long standing method for tissue or material characterization based on MRI, as T2 relaxation constant can be considered as a definite signature of the inner structure of the imaging object, used not only in medicine but in other fields such as food science, geological studies, radiation dosimetry etc. [4–6]. As opposed to water that resonates at a single frequency, lipid protons give rise to at least 8 distinct resonance peaks [7]. Each lipid spectral peak exhibits a different relaxation rate and consequently different T2 constant [8]. Estimation of T2 depends on the relevant abundance of each peak in the selected region and thus is indicative of the microscopic inner structure of the sample.

Secondly, $T2^*$ can enhance the information obtained from standard T2 relaxometry, by presenting a quantitative metric of local field inhomogeneity which is indicative of the presence of paramagnetic molecules, i.e. blood products, iron rich structures, etc. [9]. The utility of measuring $T2^*$ in combination with T2 lies on its ability to correlate well with a number of semantic physiological parameters such as local tissue oxygenation and iron concentration.

Lastly, the concept behind measuring spin coupling signal loss is based mainly on the object of this study, which is fat containing tissue. From the early days of MRI the bright appearance of fat on images with short echo spacing was reported as opposed to other structures of similar T2 relaxation constant and darker appearance [10]. Since this phenomenon is selectively observed on fat, the purpose of this study is to quantitatively evaluate signal changes for lipomatous tumors of different degree of malignancy in order to examine the clinical relevance of a novel biomarker.

Unlike water that resonates at a single frequency, fat has a complex spectrum because of its composition in different triglycerides. At clinical field strengths six distinct spectral peaks are visible at different resonant frequencies (5.3, 4.2, 2.7, 2.1, 1.3, 0.9 ppm) corresponding to different spectral components/proton moieties that collectively represent the total fat signal. The interactions through chemical bonds in the spectrum (spin coupling) result in the splitting of spectral peaks in doublets or triplets that in turn lead to signal changes of the coupled system. In particular, spin coupling evolution induces a sinusoidal modulation in addition to the T2 exponential decay of the echo train, resulting in a faster decay of the MR signal. Thus, when moving to imaging scale, fat appearance on conventional T2w Carr–Purcell–Meiboom-Gill (CPMG) images may vary significantly between different acquisition schemes, mainly depending on the time distance between consecutive 180 refocusing pulses (different ESP). Interaction between coupled spins present in fatty acid chain (hydrogen in methyl and methylene) introduce field inhomogeneities at a very local level, inducing thus an additional signal modulation to the exponential T2 decay. However, in the case of closely spaced radiofrequency pulses-small ESP- spin coupling related signal modulation

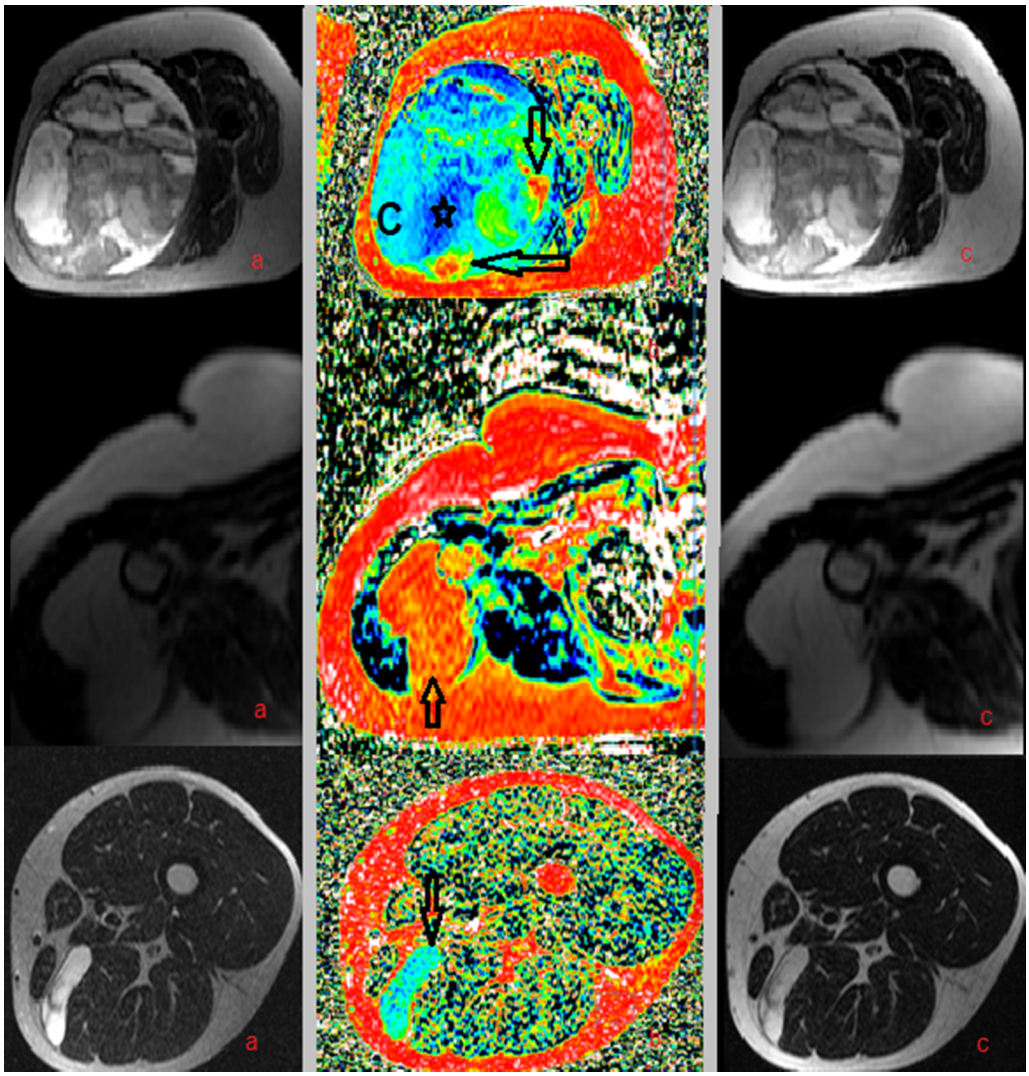

Fig. 2. SCratio maps for three lipomatous masses of variable degree of malignancy. Above: Dedifferentiated liposarcoma of the thigh: a) T2 MESE ESP: 26.8 ms, TE: 80.4 ms, b) SCr map [−10, 50] %, c) T2MESE ESP:13.4 ms TE: 80.4 ms. Histopathologic examination confirmed sites of well differentiation at the tumor periphery at locations 6o'clock and 3o' clock respectively at the periphery (arrows) that should be avoided for needle biopsy. Cystic components (C) were also observed and also sites of poor differentiation (asterisk). Fig. 2 middle: Benign Lipoma a) T2 MESE ESP: 26.8 ms, TE: 80.4 ms, b) SCr map [−10, 50, c) T2MESE ESP: 13.4 ms TE: 80.4 ms. Fig. 2 below: Myxoid Liposarcoma Lipoma a) T2 MESE ESP: 26.8 ms, TE: 80.4 ms, b) SCr map [−10, 50], c) T2MESE ESP:13.4 ms TE: 80.4 ms. All MR images are displayed at [0,1000] a.u.

(dephasing) is affected, resulting in slower relaxation rate and consequently brighter signal intensity of fat. [11]. An empirical threshold of 20 ms [12] referring to the inter pulse interval is reported, above which the fast rate of RF refocusing pulses decelerates spin coupling evolution and leads to bright fat appearance. Explicit explanation regarding the theory of multiple spin systems and the fat bi-phasic appearance can be found in references [13–15].

A phantom study from our team showed different amount of spin coupling related signal loss between oil samples of different botanical origin and thus different spectral identity, indicating that the specific inner structure of each oil sample relates to magnetic behavior of the fat and its appearance on T2w MRI [16]. The aim of the present study is to extend this research to the clinical field and examine the role of spin coupling and T2 relaxometry in supplementing pathognomonic evidence for the characterization of fat containing soft tissue masses.

2. Materials and Methods

2.1. Imaging protocol

All MRI exams were performed on a 1.5 T MR scanner (Vision/Sonata hybrid System, Siemens, Erlangen, Germany). Conventional imaging sequences presented lesion location (dual echo Proton density and T2w TSE with fat suppression) in axial and coronal plane for localization of the lesion margins (TR/TE1/TE2/TI: 3360/14/83 msec, 5 mm slice thickness/0.5 mm gap, 19 slices) and functional imaging sequences showed tumor cellularity (8-b values 2D EPI DWI TR/TE: 2900/100 msec, 5 mm slice thickness/0 mm gap, b values: 0/50/100/150/200/500/800/1500, 19 axial slices) and vascularity (a dynamic 3D T1w fast low angle shot (FLASH) (TR/TE: 7.09/3.27msec, temporal resolution 7.09 sec 5 mm slice thickness/1.6 mm gap, 14 axial slices). Imaging planes were non-oblique for easier co-localization of imaging slice and site of histological examination.

The T2 quantitative MRI protocol consists of two 2D multislice MESE, PD-to-T2-weighted sequence were obtained with no interslice delay time. For the first sequence: n = 25 equidistant spin echoes with TE_1 = 13.4 ms, ESP = 13.4 ms and for the second n = 10, TE_1 = 26.8 ms, ESP = 26.8 ms while TR was 2500 ms for both sequences.. The latter sequence (10 echoes: 26.8, …, 80.4,…, 268 ms) was used for T2 relaxometry as it does not suffer from the bright fat appearance from spin coupling while the former sequence (25 TEs: 13.4, 26.8,..,80.4,..335) was used for subtraction of images between the two relaxometry sequences at identical echo times. Fourteen axial slices of 5 mm slice thickness and 5 mm interslice distance were obtained. A rectangular field of view (280 × 210 mm) with a rectangular reconstruction matrix (256 × 192 pixels) was utilized. The final 3D spatial resolution was therefore: 1.1 × 1.1 × 8 mm^3. The MESE sequence was based on a 2D multiecho CPMG spin echo sequence with alternating 180 degrees RF pulses under the phase-alternating-phase-shift (PHAPS) scheme [17]. A selective refocusing RF pulse scheme was

Table 1
T2, T2*, Spin coupling percentage (SC) and Spin Coupling ratio (SCr) for 5 lipomas, 1 hibernoma (not included in further statistics), 4 well differentiated liposarcomas (wdls), 3 myxoid liposarcomas (mls), 2 pleomorphic liposarcomas and 4 poorly differentiated liposarcomas (pdls). Subscripts l and sf declare lesion and subcutaneous fat respectively. SCr is the ratio of spin coupling loss of the lesion over the same value of uninvolved healthy fat of the same acquisition. SD = Standard Deviation.

	T2l (ms)	T2sf (ms)	T2*l (ms)	T2*sf (ms)	SCl (%)	SCsf (%)	SCr l
lipoma 1	104,9	102,8	31,4	29,8	39,9	40,4	0,99
lipoma 2	100,4	100,9	29,2	28,0	41,3	42,0	0,98
lipoma 3	103,6	96,9	30,8	30,6	37,8	36,9	1,02
lipoma 4	102,3	99,6	28,6	29,5	38,7	36,2	1,07
lipoma 5	103,5	98,0	30,4	30,6	40,1	39,8	1,01
Mean	102,9	99,6	30,1	29,7	39,6	39,1	1,01
SD	1,5	2,1	1,0	1,0	1,2	2,2	0,03
hibernoma	196,7	96,5	103.7	29,2	−0,4	35,2	−0,01
wdls 1	103,4	99,7	44,6	29,8	36,7	39,8	0,92
wdls 2	102,5	98,7	28,8	28,5	37,1	39,7	0,93
wdls 3	101,5	98,2	31,7	29,3	49,0	51,8	0,95
wdls 4	105,5	102,0	57,3	28,4	31,9	40,3	0,79
Mean	103,2	99,7	40,6	29,0	38,7	42,9	0,90
SD	1,7	1,5	11,3	0,6	6,3	5,1	0,1
mls 1	572,0	99,5	287,0	32,0	0,2	40,5	0,00
mls 2	535,1	99,4	370,7	29,6	0,1	36,9	0,00
mls 3	383,8	100,5	282,4	28,8	7,3	41,7	0,18
Mean	497,0	99,8	313,4	30,1	2,5	39,7	0,06
SD	99,7	0,6	49,7	1,7	4,1	2,5	0,1
pls 1	144,6	100,2	78,6	28,5	6,1	34,9	0,17
pls 2	135,4	104,7	90,1	29,0	0,0	34,1	0,00
Mean	140,0	102,5	84,4	28,8	3,1	34,5	0,09
SD	6,5	3,2	8,1	0,4	4,3	0,6	0,1
pdls 1	145,4	100,7	69,3	27,1	−20,1	32,1	−0,62
pdls 2	169,3	94,9	129,5	29,5	−6,2	41,4	−0,15
pdls 3	144,3	100,5	84,4	28,8	−12,6	45	−0,28
pdls 4	131,9	99,7	59,4	30,2	−7,1	41,8	−0,17
Mean	147,7	98,9	85,6	28,9	−11,5	40,1	−0,3
SD	15,6	2,7	31,0	1,3	6,4	5,6	0,2

Table 2
Classification performance for T2, T2*, SC and SCr between lipomatous tumors. p-value is marked by "*", "**", "***", and "ns" for values between [0.01–0.05), [0.001–0.01), [0–0.001) and [0.05–1] respectively.

T2	lipoma	wdls	mls	pls	SC	lipoma	wdls	mls	pls
wdls	ns				wdls	ns			
mls	***	***			mls	***	***		
pls	ns	ns	***		pls	***	***	ns	
pdls	ns	ns	***	ns	pdls	***	***	*	ns
T2*					SCr				
wdls	ns				wdls	ns			
mls	***	***			mls	***	***		
pls	ns	ns	***		pls	***	***	ns	
pdls	ns	ns	***	ns	pdls	***	***	*	*

utilized. Additionally, a multi echo T2* MEGRE with 4 in phase echoes (4.77, 9.59, 14.41, 19.23) and 4 out of phase echoes (2.38, 7.18, 12, 16.82) was used for the calculation of T2* maps.

2.2. Data post processing

Pixel based parametric T2/T2* maps were produced after mono-exponential fitting of the multi echo MESE/MEGRE data from in-house built software platform [18]. Mean T2/T2* was calculated for each Region of Interest (ROI) which was delineated by an expert radiologist within the tumor central slice at a homogeneous region, excluding necrosis and hemorrhage. In the case of dedifferentiated liposarcoma, ROI delineation was performed after the pathologist suggested areas of poor differentiation. Image based calculations (subtraction and division of T2MESE images to calculate relative signal loss at identical TE) were performed with Mango software (Mango Software, Research Imaging Institute, UTHSCSA). Statistical analysis was performed using R. Each examined biomarker was descriptively summarized and presented as mean ± standard deviation (SD). Pairwise comparisons were assessed quantitatively using Student's T-test. Boxplots depicting the different subject groups were displayed. For all tests, a p-value of less than 0.05 was considered to indicate statistical significance.

2.3. Patient population – histological correlation

Twenty patients with lipomatous tumors underwent MRI from July 2017 to May 2018 prior to the planned surgical excision. One patient was excluded because of compromised cooperation resulting in severe motion artifacts. All patients signed an informed consent for the use of clinical and imaging data for research purposes. Surgeon marked the specimen with sutures in predefined points in order to enable the actual three-dimensional orientation of the specimen in relation with the patient's body and to warrant the implementation of sections of the tumor in its true axial plane. The intact surgical specimen was transported promptly to the pathology department, were it was delivered to and handled by a trained pathologist who performed the gross examination, photographed and marked the specimen with permanent ink according to the surgical markings and margins. Furthermore, after identifying the upper and lower margins of the tumor, in the superior-inferior direction, parallel sections perpendicular to the axial plane of 1 cm thickness were taken. The central slice of the tumor, corresponding to the lesion's central imaging slice, was selected after measuring the distances from the upper and lower margins, was divided in orthogonal slabs (in a grid-manner), and placed into plastic cassettes (Fig. 1). Tumor tissue sections were processed according to CAP guidelines and recommendations for specimen handling [19]. In brief after 48 h' fixation into 10% neutral buffered formalin, sections were embedded into paraffin, dehydrated through a series of graded ethanol baths, infiltrated with wax and then embedded into wax blocks. 4 μm thick

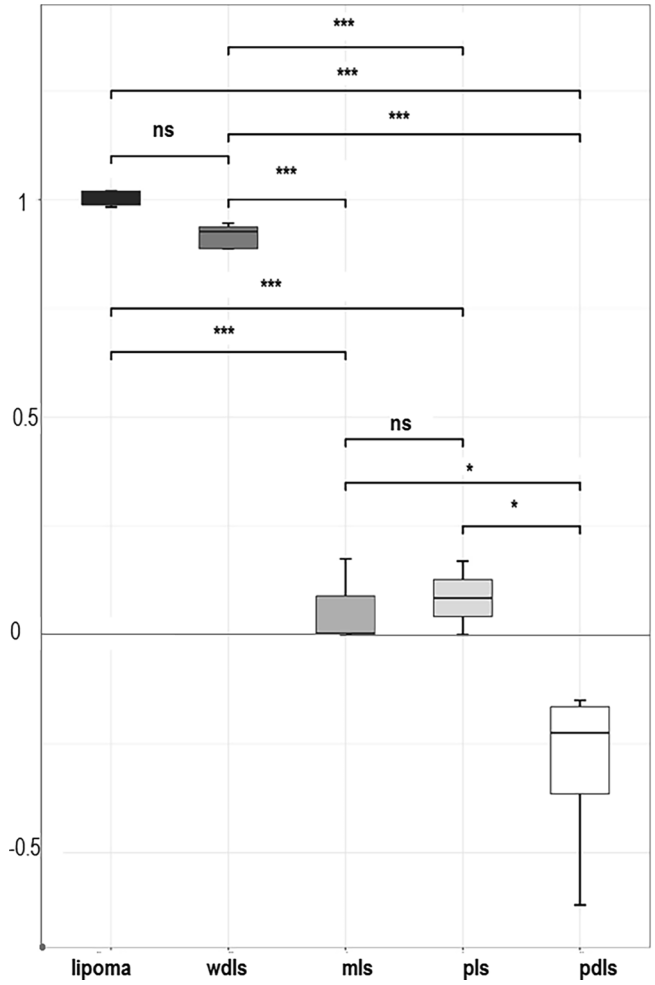

Fig. 3. Box plot graphically representing mean value and standard deviation for each category based on SCr. for all lipomatous tumor types. p-value is marked by "*", "**", "***", and "ns" for values between [0.01–0.05), [0.001–0.01), [0–0.001) and [0.05–1] respectively.

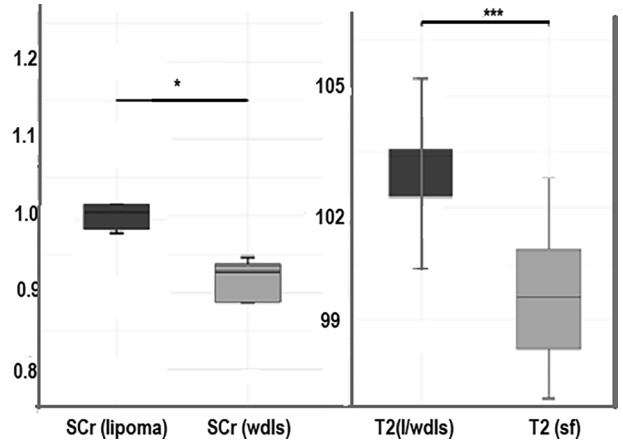

Fig. 4. Classification problem simplified to two categories. Left: Significant difference is found between lipoma and well differentiated liposarcoma based on SCr. Right: Lipoma or well differentiated liposarcoma have significant differences in measured T2 value from uninvolved subcutaneous fat (sf).

sections of each tumor slab were cut, placed into glass slides, stained with H/E and examined microscopically (Nikon Eclipse E-200) in order to characterize each area of the central tumor slice in terms of differentiation, cell type, cellular atypia, cellularity, mitotic activity, vascularity and presence of necrosis.

The histopathologic topographic characterization guided the imaging post-processing stage so as to recognize the histologically designated "benign", "necrotic", malignant areas and also to conclude on differentiation grade on a very locally restricted area which could be used for ROI measurements. The corresponding site was located on the central imaging slice as distance from the center and angle in a virtual axially located 360 degree cycle.

A case of hibernoma was included in the patient cohort because of its interest but was not included in the statistical analysis as it cannot constitute a category by itself. Data from patients diagnosed with dedifferentiated liposarcoma were assigned as either well or poorly differentiated tissue according to the result of histological examination for the selected slice.

The relative signal loss percentage of the fatty tissue between two T2 acquisitions of different echo spacing, 13.4 ms and 26.8 ms respectively was calculated (Spin Coupling, SC) for all image pixels (Eq. (1)).

$$SC = \frac{T2_1 - T2_2}{T2_1} \quad (1)$$

SC value calculated for the tumor ROI was then divided by SC value calculated for subcutaneous fat ROI of the same patient from the same acquisition in order to produce a patient specific metric, Spin Coupling ratio, (SCr) (Eq. (2)).

$$SC_{ratio} = \frac{SC_{tumor}}{SC_{fat}} \quad (2)$$

3. Results

Resulting pixel based parametric maps of SCr are shown on Fig. 2, complemented by original bright and dark fat T2w images, ROI based mean apparent T2, mean apparent mean $T2^*$ were calculated for the lesion as well as for uninvolved fat adjacent to the tumor volume to be used as reference for protocol robustness (Table 1). Subcutaneous fat sustains a relatively constant value for mean apparent $T2/T2^*$ within the patient population, unlike fat containing tumors that exhibit an extensive range of values. Similarly SCr remains relatively constant for healthy fat among all patients while there is a significant range of measured values between different types of fat containing neoplasms.

Statistical analysis (pairwise *t*-test with Bonferroni correction) was performed to find significant differences in mean apparent T2, mean apparent $T2^*$ and SCr between five distinct categories, i.e lipoma, well differentiated liposarcoma, myxoid liposarcoma, pleomorphic liposarcomas and poorly differentiated liposarcoma. Difference was considered significant for p less than 0.05, and is marked by * for p between [0.01–0.05), ** for p [0.001–0.01) and lastly marked with *** for p between [0–0.001) as shown in Table 2. Non-significant differences are noted as ns. Fig. 3 graphically represents SCr results, as this was proved (from results shown on Table 2) the metric with the higher discriminative power among all three.

It is of note that only SCratio succeeded in classification between pleomorphic liposarcoma and poorly differentiated part of dedifferentiated liposarcoma, both of which are graded as highly malignant (histologic specific grade: 3) and have similar imaging characteristics.

No metric could find significant differences between lipoma and well differentiated liposarcoma in the 5-class problem. However, when performing a 2-class classification between the two classes of low malignancy and very similar imaging characteristics, SCr shows significant differences between lipoma and well differentiated liposarcoma while all the other metrics fail (Fig. 4 left).

Furthermore a pairwise *t*-test was performed between an "extended" class including two entities (lipoma and well differentiated liposarcoma) tested versus healthy subcutaneous fat visible in the same acquisition based on T2 relaxation constant. Significant differences are found between tumors and normal appearing adjacent fatty tissue

(Fig. 4 right).

4. Discussion

Fat quantification and fat content determination has been a long standing target of quantitative MRI. To our knowledge, the first use of spin coupling as contrast for clinical imaging was published in 1993 [20].

Currently, the most widely used NMR based method for the study of tissue structure is in vivo MR spectroscopy. It offers direct recognition of each spectral peak and its relative amplitude for a given sample, but it is has many inherent constraints that prevent extensive use in a routine basis. It requires special software and post processing, human expertise, adequate sample homogeneity and main field homogeneity. Ex-vivo 13C MRS has been used by S. Singer et al to differentiate between fat-containing tumors based on tissue biochemistry [21]. The major findings of this study were significant differences in the fatty acyl chain content (ratio between lipomas: wdls: pls or dediff. liposarcomas is 1 : 3 : 0.01) probably attributed to the increase of the poly-unsaturation degree of high grade sarcomas as compared to intermediate or low grade. The latter suggests an increase in the number of double bonds present in the fatty acyl chain which affects the motion and order of the acyl chain and in turn affects membrane proteins. This can be an important factor determining the invasive and metastatic capacity of the high grade liposarcoma cell types. Moreover they remarked the presence of free fatty acids and phospholipids in dedifferentiated/pleomorphic sarcomas which were not detectable in normal fat, lipoma or well differentiated liposarcoma.

The proposed method based on spin coupling ratio does not rely on direct detection of tissue composition but taking into account the biochemical differences observed in the spectrum, changes in lipid specific imaging contrast are expected. Differences in the measured SCr show variable degree of dependence on refocusing pulse spacing and may be indicative of differences in the fat content of adipocytic neoplasms. Subcutaneous fat exhibits a very narrow and specific range of all T2 and Spin Coupling related metrics instead in the resulting changes of signal produced. SCr calculation does not require special hardware or software nor post processing expertise. It requires minimal acquisition time and has excellent spatial resolution, exploiting rather than being weakened by tissue heterogeneity as in the case of MR spectroscopy.

Results of the present study show that T2 relaxometry in conjunction with spin coupling ratio can achieve differentiation between any pair of the five different adipocytic moieties. As seen in Fig. 3 SCr decreases with increased differentiation grade. Well differentiated liposarcomas lose a significant percentage (38.9%) of their signal due to spin coupling at TE = 80 ms which is comparable to normal fat signal loss (42.9%), myxoid have almost identical signal intensity between the two acquisitions-probably because of the dominant long T2 component-and, at the other end, pleomorphic and poorly differentiated tumors have even lower SCr. In fact, the latter group exhibits negative values which was unexpected as zero loss was considered to be the lower limit by theory. However this finding was consistent among all examined patients and requires more detailed study in a molecular and chemical level.

In FSE each echo has a distinct phase encoding in order to represent a different line of k-space within a given TR interval. The effect of spin coupling in signal modulation cannot be decomposed and measured separately to other concurrent spin dephasing phenomena during acquisition, such as magnetization exchange effects, stimulated echoes or diffusion of water molecules through a local field inhomogeneities [22]. However, the process of subtraction of images with identical parameters apart from ESP accentuates contrast mechanisms affected significantly by pulse spacing. For this reason, we believe that, if not uniquely, the observed differences can be attributed mainly to spin coupling.

A definite constrain of our study is the number of patients that participated in the study but these preliminary results show that SCr can be introduced into the clinical routine and to build a larger database for use in the future. However it is promising that structures of similar origin but different molecular inner structure or composition have a different imaging identity and the proposed biomarker of spin coupling ratio highlights the imaging spectrum of fat that remains otherwise unperceivable.

In conclusion, the novel biomarker SCr can be introduced as a quantitative adjunct for radiological assessment of lipomatous tissue type and grade with minimal software and time prerequisites. Clinical implications of this MRI technique may be biopsy guidance in heterogenous lipomatous tumors to assure for harvesting tissue with the highest malignancy grade and non-invasive preoperative diagnosis of tumor type and grade, which is essential for adequate treatment planning.

References

[1] Nassif NA, Tseng W, Borges C, Chen P, Eisenberg B. Recent advances in the management of liposarcoma. F1000Res 2016;5:2907https://doi.org//10.12688/f1000research.10050.1.

[2] Gupta P, Potti TA, Wuertzer SD, Lenchik L, Pacholke DA. Spectrum of fat-containing soft-tissue masses at mr imaging: the common, the uncommon, the characteristic, and the sometimes confusing. RadioGraphics 2016;36:753–66. https://doi.org/10.1148/rg.2016150133.

[3] Nishida J, Morita T, Ogose A, Okada K, Kakizaki H, Tajino T, et al. Imaging characteristics of deep-seated lipomatous tumors: intramuscular lipoma, intermuscular lipoma, and lipoma-like liposarcoma. J Orthop Sci 2007;12:533–41. https://doi.org/10.1007/S00776-007-1177-3.

[4] Santos PM, Vinicius F, Kock C, Santos MS, Lobo CMS, Carvalho AS, et al. Non-invasive detection of adulterated olive oil in full bottles using time-domain NMR relaxometry. Artic J Braz Chem Soc 2017;28:385–90. https://doi.org/10.5935/0103-5053.20160188.

[5] Loskutov V, Zhakov S. Dependence of the liquid transverse relaxation time T2 in porous media on fluid flow velocity. Int J Heat Mass Transf 2016;101:692–8. https://doi.org/10.1016/J.IJHEATMASSTRANSFER.2016.05.057.

[6] Maris TG, Pappas E, Boursianis T, Kalaitzakis G, Papanikolaou N, Watts L, et al. 3D polymer gel MRI dosimetry using a 2D haste, A 2D TSE AND A 2D SE multi echo (ME) T2 relaxometric sequences: Comparison of dosimetric results. Phys Medica 2016;32:238–9. https://doi.org/10.1016/J.EJMP.2016.07.498.

[7] Brix G, Heiland S, Bellemann ME, Koch T, Lorenz WJ. MR imaging of fat-containing tissues: valuation of two quantitative imaging techniques in comparison with localized proton spectroscopy. Magn Reson Imaging 1993;11:977–91. https://doi.org/10.1016/0730-725X(93)90217-2.

[8] Hamilton G, Smith DL, Bydder M, Nayak KS, Hu HH, Hu HH. MR properties of brown and white adipose tissues. J Magn Reson Imaging 2011;34:468–73. https://doi.org/10.1002/jmri.22623.

[9] He T, Gatehouse PD, Smith GC, Mohiaddin RH, Pennell DJ, Firmin DN. Myocardial $T2^{*}$ measurements in iron-overloaded thalassemia: An in vivo study to investigate optimal methods of quantification. Magn Reson Med 2008;60:1082–9. https://doi.org/10.1002/mrm.21744.

[10] Hardy PA, Henkelman RM, Bishop JE, Poon ECS, Plewes DB. Why fat is bright in rare and fast spin-echo imaging. J Magn Reson Imaging 1992;2:533–40. https://doi.org/10.1002/jmri.1880020511.

[11] Yahya A, Tessier AG, Fallone BG. Effect of J-coupling on lipid composition determination with localized proton magnetic resonance spectroscopy at 9.4 T. J Magn Reson Imaging 2011;34:1388–96. https://doi.org/10.1002/jmri.22792.

[12] Stables LA, Kennan RP, Anderson AW, Gore JC. Density matrix simulations of the effects of j coupling in spin echo and fast spin echo imaging. J Magn Reson 1999;140:305–14. https://doi.org/10.1006/JMRE.1998.1655.

[13] Hennig J, Thiel T, Speck O. Improved sensitivity to overlapping multiplet signals in in vivo proton spectroscopy using a multiecho volume selective (CPRESS) experiment. Magn Reson Med 1997;37:816–20. https://doi.org/10.1002/mrm.1910370603.

[14] Allerhand A, Thiele E. Analysis of carr—purcell spin-echo nmr experiments on multiple-spin systems. II. The effect of chemical exchange. J Chem Phys 1966;45:902–16. https://doi.org/10.1063/1.1727703.

[15] de Graaf RA, Rothman DL. In vivo detection and quantification of scalar coupled1H NMR resonances. Concepts Magn Reson 2001;13:32–76. https://doi.org/10.1002/1099-0534(2001) 13:1<32::AID-CMR4>3.0.CO;2-J.

[16] Nikiforaki K, Manikis GC, Boursianis T, Marias K, Karantanas A, Maris TG. The impact of spin coupling signal loss on fat content characterization in multi-echo acquisitions with different echo spacing. Magn Reson Imaging 2017;38. https://doi.org/10.1016/j.mri.2016.12.011.

[17] Fransson A, Ericsson A, Jung B, Sperber GO. Properties of the PHase-Alternating Phase-Shift (PHAPS) multiple spin-echo protocol in MRI: a study of the effects of imperfect RF pulses. Magn Reson Imaging 1993;11:771–84. https://doi.org/10.1016/0730-725X(93)90195-J.

[18] Manikis GC, Nikiforaki K, Papanikolaou N, Marias K. Diffusion Modelling Tool (DMT) for the analysis of Diffusion Weighted Imaging (DWI) Magnetic Resonance

Imaging (MRI) data. Proc. 33rd Comput. Graph. Int. – CGI '16 New York, New York, USA: ACM Press; 2016. p. 97–100. https://doi.org/10.1145/2949035.2949060.
[19] Lester SC. Manual of surgical pathology. Saunders/Elsevier 2010.
[20] Todd Constable R, Smith RC, Gore JC. Coupled-spin fast spin-echo MR imaging. J Magn Reson Imaging 1993;3:547–52. https://doi.org/10.1002/jmri.1880030319.
[21] Singer S, Millis K, Souza K, Fletcher C. Correlation of lipid content and composition with liposarcoma histology and grade. Ann Surg Oncol 1997;4:557–63. https://doi.org/10.1007/BF02305536.
[22] Constable RT, Anderson AW, Zhong J, Gore JC. Factors influencing contrast in fast spin-echo MR imaging. Magn Reson Imaging 1992;10:497–511. https://doi.org/10.1016/0730-725X(92)90001-G.